ACS OMEGA

http://pubs.acs.org/journal/acsodf

Article

Stability Mechanism of Low Temperature C_2H_4−SCR with Activated-Carbon-Supported MnO_x-Based Catalyst

Fang Liu,* Jiangyuan Zhao, Shengbao He, Qing Liu, Guangli Liu, and Li Yang

Cite This: *ACS Omega* 2022, 7, 12004−12014

Read Online

ACCESS | Metrics & More | Article Recommendations

ABSTRACT: Manganese-based catalysts have shown great potential for use as a hydrocarbon reductant for NO_x reduction (HC-SCR) at low temperatures if their catalytic stability could be further maintained. The effect of CeO_2 as a promoter and catalyst stability agent for activated carbon supported MnO_x was investigated during low temperature deNO_x based on a C_2H_4 reductant. The modern characterization technology could provide a clear understanding of the activity observed during the deNO_x tests. When reaction temperatures were greater than 180 °C and with ceria concentrations more than 5%, the overall NO conversion became stable near 70% during long duration testing. In situ DRIFTS shows that C_2H_4 is adsorbed on the Mn_3Ce_3/NAC catalysts to generate hydrocarbon activated intermediates, R-COOH, and the reaction mechanism followed the E-R mechanism. The stability and the analytical data pointed to the formation of stable oxygen vacancies within Ce^{3+}/Ce^{4+} redox couplets that prevented the reduction of MnO_2 to crystalline Mn_2O_3 and promoted the chemisorption of oxygen on the surface of MnO_x-CeO_x structures. Based on the data, a synergetic mechanism model of the deNO_x activity is proposed for the MnO_x-CeO_x catalysts.

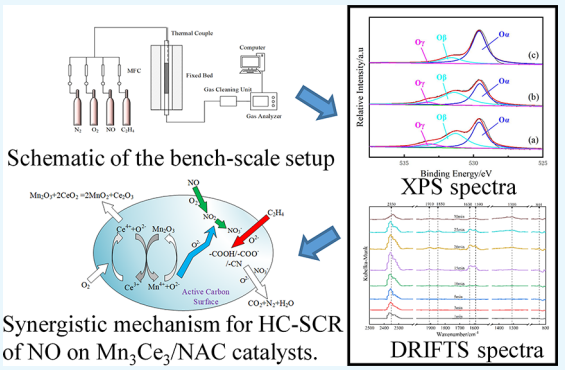

1. INTRODUCTION

Large amounts of NO_x emissions into the atmosphere lead to photochemical smog and chemical and eutrophication.[1−3] Hence, NO_x emission standards are becoming more rigorous, and NO_x reduction technologies, such as NO_x direct decomposition, selective noncatalytic reduction (SNCR), and selective catalytic reduction (SCR), have become more intensely investigated;[4−6] of these, SCR is the most diffusely used technology to control NO_x emission. The most established, commercial strategy for abating NO_x emissions during SCR is to use NH_3 as the reductant,[7−10] and commercial catalysts are based mainly on V_2O_5−WO_3/TiO_2.[11−13] Ammonia is expensive; requires special handling, transport, storage, and application systems; and requires sophisticated metering to minimize NH_3 slip.[14,15] NH_3 slip causes plugging of ducts downstream of air-preheaters, forms secondary, fine particulate that is emitted into the atmosphere, and is regarded as an air pollutant potentially more objectionable than NO_x.[16,17] In addition, spent vanadium-based catalyst is classified as a detrimental solid waste, and its post processing is also costly.[18,19]

In contrast with NH_3, hydrocarbons (HC) like C_2H_4 and C_3H_8 have low cost, high reducibility, user-friendliness, widespread distribution, and no NH_3 slip, and most importantly, they are byproducts in the refinery station,[20] so they can be directly used to reduce the NO_x in the refinery station instead of long distance transportation and storage. Furthermore, hydrocarbons (HC) do not suffers from fouling by salt deposition, and some refinery stations have already used hydrocarbons (HC) to reduce NO_x. The overall Hydrocarbon-SCR reaction equation is as follows:

$$C_xH_y + 2NO + (x + 0.25y - 1)O_2 = N_2 + xCO_2 + 0.5yH_2O \quad (1)$$

In addition, vanadium-based NH_3−SCR operates in a narrow temperature window of 350−420 °C.[13] Hence, they are always used ahead of dust catcher and desulfurization systems to fulfill the desired temperature windows without extra heating. However, the presence of SO_2 and dust in these process locations reduces catalyst performance and durability.[21,22] Nevertheless, if the running temperature could be reduced to, for instance, less than 250 °C, then de-NO_x facilities could be installed downstream of heat recovery steam generators (HRSG). Importantly, small-scale industrial boilers, such as steel furnaces, glass kilns, and coke ovens,

Received: January 10, 2022
Accepted: March 9, 2022
Published: March 24, 2022

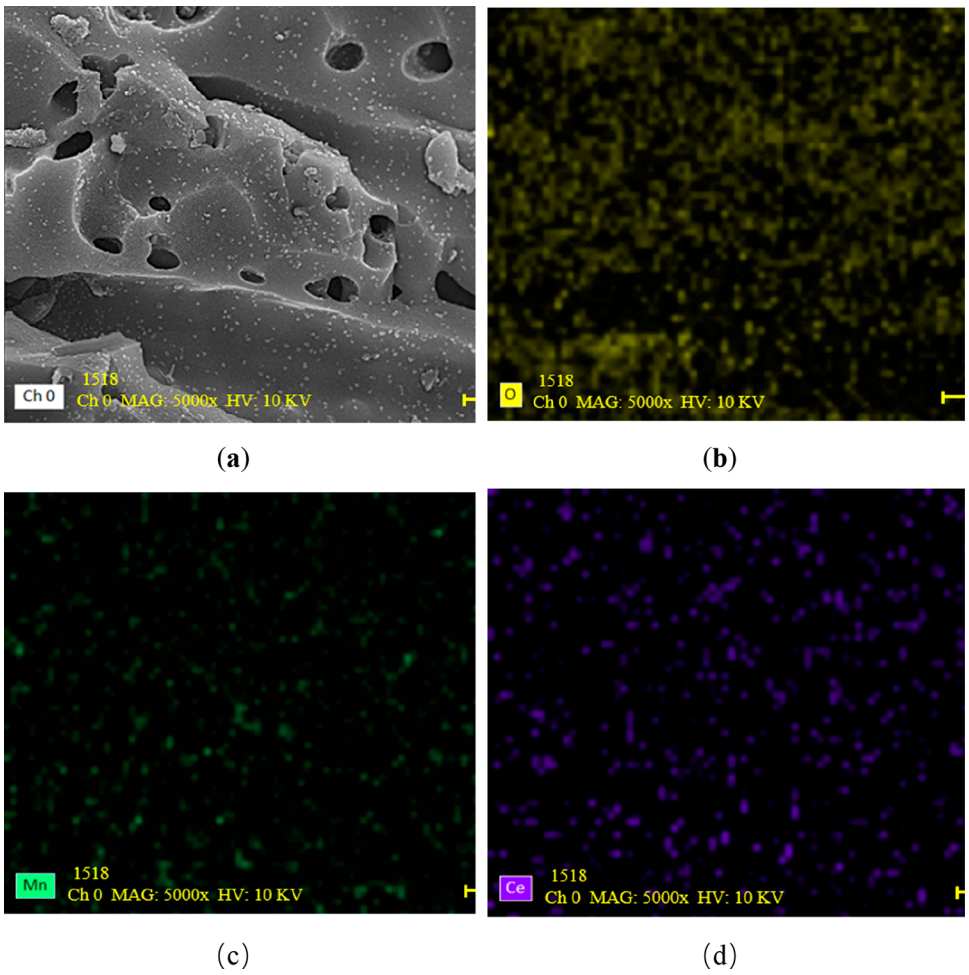

Figure 1. SEM and EDS images of Mn_3Ce_3/NAC: (a) SEM image Mn_3Ce_3/NAC SEM, 5000×; (b) EDS mapping of O; (c) EDS mapping of Mn; (d) EDS mapping of Ce.

operate with flue gas temperatures about 200−300 °C[23−25] and temperatures of desulfurization units below 200 °C. Under these conditions, vanadium-based catalysts would not be effective.[26,27] Thereby, developing effective and stable catalysts using low-temperature (<200 °C) HC-SCR has become a scientific and development quest with important practical implications.[24]

Among various catalyst active components investigated for HC-SCR of NO_x, noble metals have shown promising results;[28] for example, an Ag−Mg−Al composition (Ag_7MgAl) at 350 °C exhibited 98% NO conversion. In general, however, noble metals have high costs, limiting their application in large-scale commercial operations; they are also not applicable for low-temperature HC-SCR reactions because their reactivities require temperatures near or higher than 350 °C. With concerns of low-temperature operating conditions, transition metal oxides served as potential candidates for HC-SCR catalysis because of their reactivity, low cost, and environmental acceptance.[29,30] For example, NO conversion was reported while using Cu/ZSM-5 with C_3H_6 as a reductant;[31] MnO_x is known for its initial, high reactivity at low temperatures for HC-SCR reactions.[32] Supports, such as Al_2O_3,[33] TiO_2,[34] SiO_2,[35] and activated carbon (AC),[36] have been used with MnO_x-based catalysts. Both SiO_2 and TiO_2 have demonstrated thermostability and acceptable mechanical capacities, while AC presents high surface area and porosity that imply the possibility of readily dispersing the active metal oxide and enabling reactant access to the active sites;[37,38] however, most of these studies have used NH_3 as the reductant.[39]

MnO_x/AC[40] was used with C_2H_4 as a reductant and exhibited over 90% NO conversion even at temperatures as low as 130 °C; it deactivated rapidly such that only 20% conversion was evident after only 2 h of testing. This deactivation was attributed to a combination of the following: first, the valence state of the Mn decreased from Mn^{4+} to Mn^{3+} and Mn^{2+}, but Mn^{4+} was found to be more active than the other two valences; second, carbon black was deposited on the active carbon surface during SCR reaction testing, blocking channels, and active catalytic sites. Cerium oxides (CeO_2) have a specific fluorite structure, in which with each Ce^{4+} is surrounded by eight equivalent, nearest O^{2-} ions which formed the corners of a cube structure and coordinated to four Ce^{4+} ions.[41] The ion configuration contributes to a high oxygen storage capacity, a vast number of oxygen vacancies, and strong redox properties between Ce^{3+} and Ce^{4+}, which may help maintain the stability of MnO_2. Therefore, ceria as an additive was considered a strong candidate to help promote and maintain the catalytic performance of MnO_x-based catalysts during HC-SCR reaction testing at low temperatures.[42−44] Characterization data shows that there were a number of oxygen defects produced by $Mn^{3+} + Ti^{4+} \leftrightarrow Mn^{4+} + Ti^{3+}$ and

https://doi.org/10.1021/acsomega.2c00202
ACS Omega 2022, 7, 12004−12014

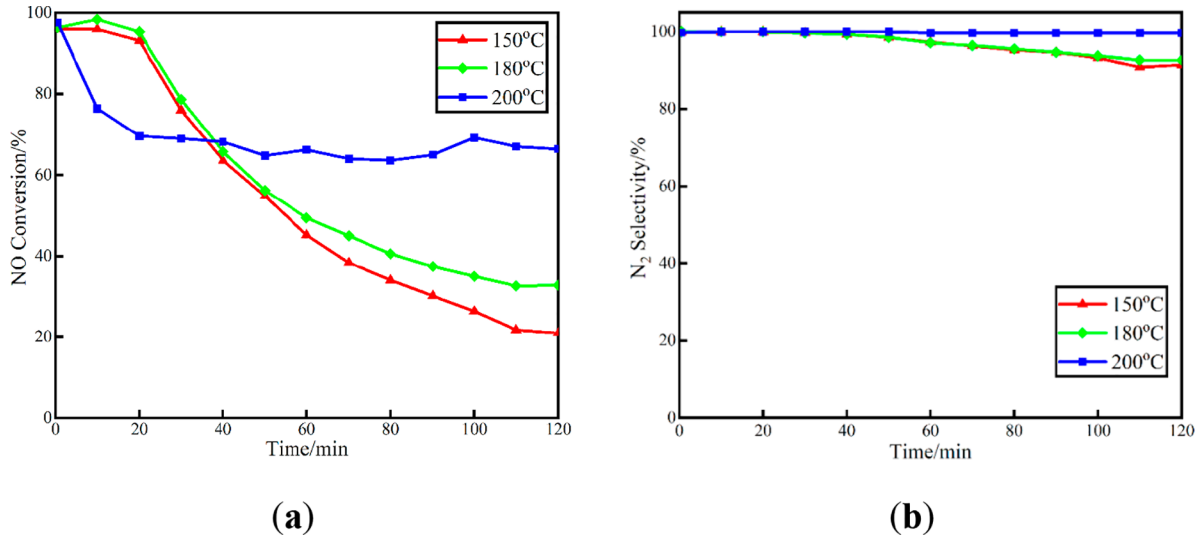

Figure 2. (a) NO conversion. (b) N_2 selectivity of Mn_3Ce_3/NAC using C_2H_4 as a reductant. Reaction temperature varied from 150 to 200 °C; reaction conditions were 500 ppm of NO, 250 ppm of C_2H_4, and 3% O_2 with a flow rate of 1500 mL/min.

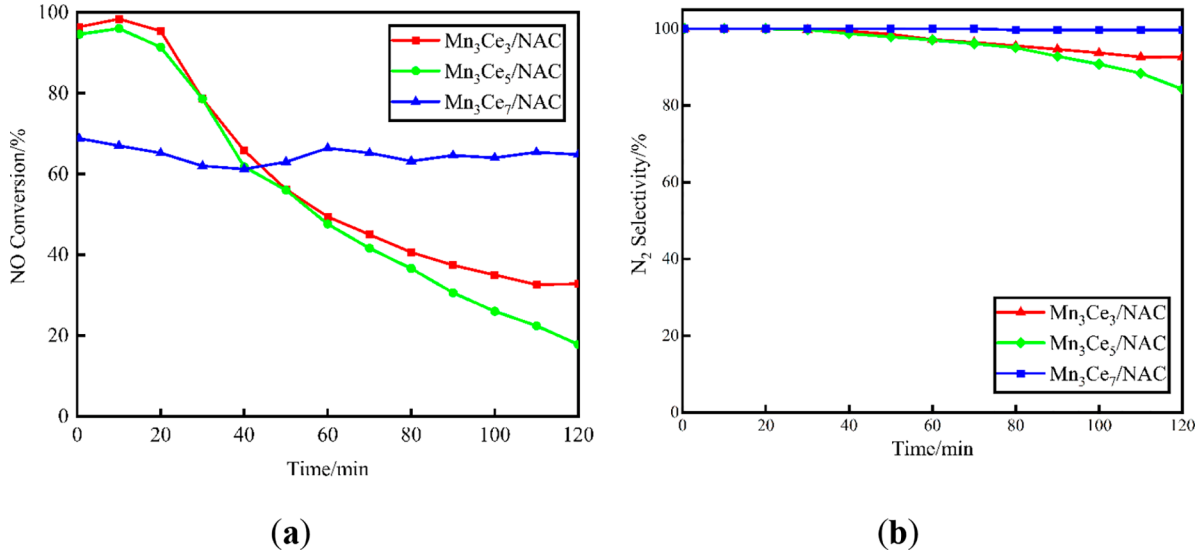

Figure 3. (a) NO conversion and (b) N_2 selectivity of Mn_3Ce_x/NAC (x = 3, 5, 7) used C_2H_4 as a reductant. Reaction temperature was 180 °C, and the reaction conditions were 500 ppm of NO, 250 ppm of C_2H_4, and 3% O_2 with a flow rate of 1500 mL/min.

$Ce^{4+} + Mn^{3+} \leftrightarrow Ce^{3+} + Mn^{4+}$, which was a beneficial improvement of $deNO_x$, these two reactions generated a charge imbalance, oxygen vacancies, and unsaturated chemical bonds on the catalyst surface.[45,46]

This study will investigate the catalytic performance of ceria modified Mn/AC catalysts, and further explore the promotion mechanism of CeO_2, which could help develop stable and highly active HC-SCR catalysts. The effect of CeO_2 as a promoter and a catalyst stability agent for activated carbon supported MnO_x will be investigated during low temperature $deNO_x$ based on C_2H_4 reductant. The modern characterization technology could provide a clear understanding of the activity observed during the $deNO_x$ tests.

2. RESULTS AND DISCUSSION

2.1. Dispersion of Active Component. SEM images and EDS elemental mappings of fresh Mn_3Ce_3/NAC catalyst are presented in Figure 1. The catalyst morphology was similar to that in previous studies,[40] the active components are evenly loaded on the surface of the activated carbon with particle structure. Elemental distributions indicated well-dispersed manganese and cerium on the NAC surface and without agglomeration,[47] which helps to improve the catalytic efficiency of the catalyst.

2.2. Catalytic Performance. Figure 2a shows the HC-SCR catalytic performance of Mn_3Ce_3/NAC at 150, 180, and 200 °C. Similar to MnO_x/NAC without CeO_x,[20] excellent NO conversion was observed at 150 and 180 °C during the first 20 min of testing, but large decreases in NO conversion then occurred, such that only about 20% NO conversion remained after 2 h of reaction testing. In contrast, at 200 °C after an initial sharp drop in conversion, the activity was constant at 65% over the entire 2 h period of testing. This may be because at the initial stage of the reaction, most of Mn and Ce in the fresh catalyst are in the forward direction in the catalytic reduction reaction, but the reaction is not balanced at this time. After the chemical reaction is in equilibrium, the NO conversion rate tends to be stable, and the valence state

https://doi.org/10.1021/acsomega.2c00202
ACS Omega 2022, 7, 12004−12014

changes of Mn and Ce in the catalyst also tend to be stable. N_2O less than 2 ppm was measured by GC to, so it was not discussed in this study. The N_2 selectivity of Mn_3Ce_3/NAC is shown in Figure 2b; as can be seen, it could remain at a high level for above 90%, especially for reaction at 200 °C, where the N_2 selectivity reached 100% during overall reaction time.

Effects of the Ce loading on NO conversion and N_2 selectivity at 180 °C were investigated (Figure 3). The NO conversion times for Mn_3Ce_3/NAC and Mn_3Ce_5/NAC were very similar to the results from Mn_3Ce_3/NAC as shown in Figure 2a when the reaction temperatures were either 150 or 180 °C. However, when the Ce loading was increased to 7% and the reaction temperature was 180 °C, the NO conversion rate remained stable over the entire period of the testing. By comparing the data in Figure 2a and Figure 3a, it was concluded that both reaction temperatures and CeO_x concentrations can affect NO conversion rates and stabilities during HC-SCR.

The presence of CeO_x has been shown to be capable of mitigating the deactivation of Mn_x/NAC catalysts during low temperature HC-SCR reaction testing.[40] Hence, physical and chemical differences in MnCe/NAC catalysts were investigated before and after reaction testing to shed light on changes which may affect NO conversion rates.

2.3. Promoting Mechanism of Ce Loading. *2.3.1. Effect of Ce Addition on the Surface Area.* As displayed in Table 1, the BET surface areas were decreased by about 15% upon impregnating CeO_x onto a MnO_x/NAC catalyst, but its surface area was not significantly different after reaction testing; these results suggest that MnO_x and CeO_x had minimal influence on the textural properties and the surface structure of the catalyst.[48] Although the larger surface area is known to be beneficial to the chemical reactivity of HC-SCR reactions,[49] it was not the key to affecting the catalytic activity of Mn_3Ce_3/NAC, because the decrease of catalytic performance was more drastic than the change of surface area.

Table 1. Specific Surface Area

samples	BET surface area (m^2/g)
Fresh AC	439.07
Mn_3 /NAC Before Reaction	668.54
Mn_3Ce_3/NAC Before Reaction	599.35
Mn_3Ce_3/NAC After 150 °C Reaction	547.72
Mn_3Ce_3/NAC After 200 °C Reaction	571.40

2.3.2. Morphology Evolution. The SEM/EDS images in Figure 4 and Figure 5, respectively, display morphologies and sizes of the Ce-rich and Mn-rich particles of Mn_3Ce_3/NAC after HC-SCR reaction testing at 150 and 200 °C. During the experiment, the state of the activated carbon support did not change significantly before and after the reaction. As compared to the as-prepared catalyst, reaction testing caused growth in the sizes of both Mn- and Ce-rich particles, but the EDS data also suggest that the Mn was more highly dispersed after 200 °C testing than after 150 °C testing. This difference may be related to an increased probability of interactions between Ce and Mn which enabled continued, stable NO conversion at 200 °C as opposed to the steady decrease in NO conversion at 150 °C.

2.3.3. Crystalline Phases. Figure 6 data show the XRD patterns of Mn_3Ce_3/NAC tested at 200 °C were very similar before and after reaction testing, whereas while the XRD pattern of the catalyst tested at 150 °C was different, the intensity of XRD peaks for the sample after the reaction at 150 °C decreased. Interpreting the exact contributions to peak intensities from the various compounds was complicated, because it required deconvolution of overlapping peaks due amorphous carbon, CeO_2, MnO_2 and Mn_3O_4. However, if the intensity contributions from amorphous carbon to the peak at 2θ = 24° and 2θ = 43° were approximately constant—as indicated by the fact that the peak intensity from carbon at 2θ = 43° was mostly unchanged independent of whether the fresh catalysts tested at 150 or 200 °C were examined—then the overall intensity changes in the 2θ = 20−30° composite peak were primarily caused by differences in concentrations and/or crystallinities of the metal oxides. In addition, the intensity of the CeO_2 peak at 79.1° was slightly less in the fresh than in catalyst tested at 200 °C, indicating different crystallinity for CeO_2 in the catalyst tested at 150 °C; as a consequence, it would contribute to distinct shoulders in peak intensities at 28.5°, 47.5°, and 56.3°. Simultaneously, the peak at 56.3° was most pronounced in the catalysts tested at 200 °C, thereby implying that the concentration and/or crystallinity of MnO_2 was distinct in the catalysts tested at 200 °C as compared to the other tested catalysts. Therefore, the MnO_2 and CeO_2 components of the catalysts tested at 200 °C were more stable than those tested at 150 °C. This stability in the crystalline

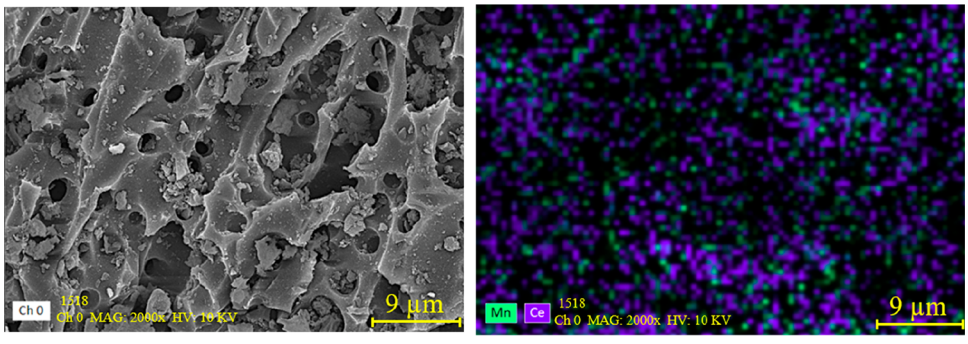

(a) (b)

Figure 4. Morphology of Mn_3Ce_3/NAC after reaction testing of 150 °C. (a) SEM image Mn_3Ce_3/NAC, 2000×. (b) EDS image of Mn/Ce element dispersion.

https://doi.org/10.1021/acsomega.2c00202
ACS Omega 2022, 7, 12004−12014

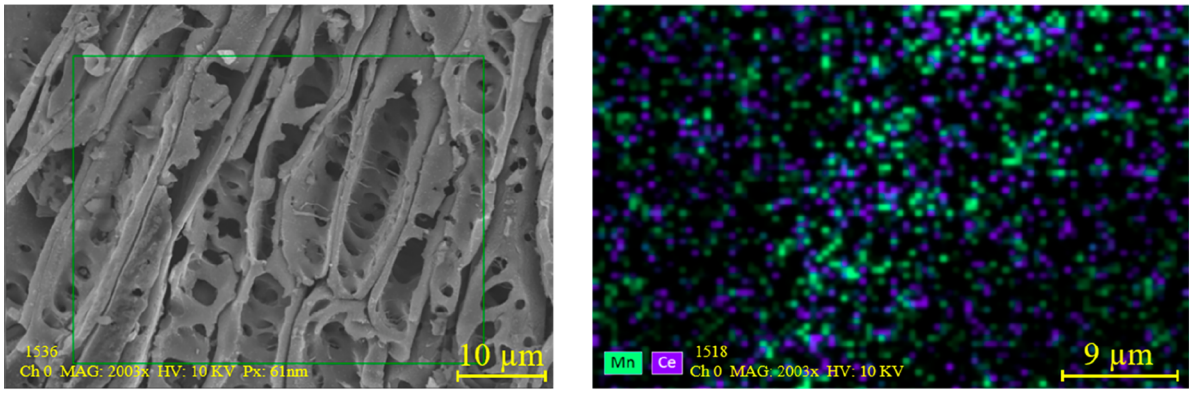

Figure 5. Morphology of Mn_3Ce_3/NAC after reaction testing of 200 °C. (a) SEM image Mn_3Ce_3/NAC, 2003×. (b) EDS image of Mn/Ce element dispersion.

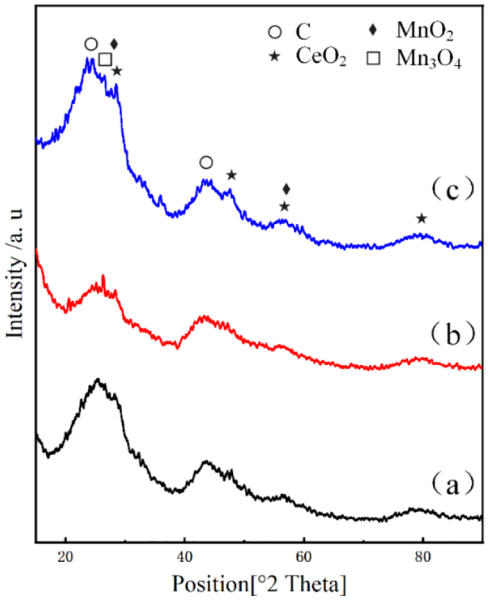

Figure 6. XRD pattern of Mn_3Ce_3/NAC catalyst: (a) before reaction testing; (b) after 150 °C reaction testing; (c) after 200 °C reaction testing.

phase may enable the catalysts tested at 200 °C to maintain the oxidation state of Mn and its catalytic performance.

2.3.4. H_2-TPR Analysis. The H_2-TPR data shown in Figure 7 exhibited a TPR profile that was deconvoluted into three distinct peaks between 200 and 800 °C.[50] Reduction of the weakest Mn−O bonds occurred at the temperature region T_1 and was for MnO_2 to Mn_2O_3; the amorphous Mn_2O_3 was then reduced to Mn_3O_4 before converting to MnO at temperature T_2. The reduction of CeO_2 was mainly concentrated between 518 and 787 °C and assigned to the T_3 temperature.[51]

Before reaction testing, the two main reduction peaks were at 442 and 644 °C, in which the 442 °C peak was attributed to Mn_2O_3 and the peak at 644 °C was assigned to surface reduction of CeO_2; the 442 °C peak could accounted for reduction of surface Ce^{4+} to Ce^{3+}.[52] For the 150 °C reaction tested sample, the intensity of the 442 °C peak was greater than before testing, indicating more Mn_2O_3 after testing.[53] From the literature,[54] it is expected that the reduction of MnO_x

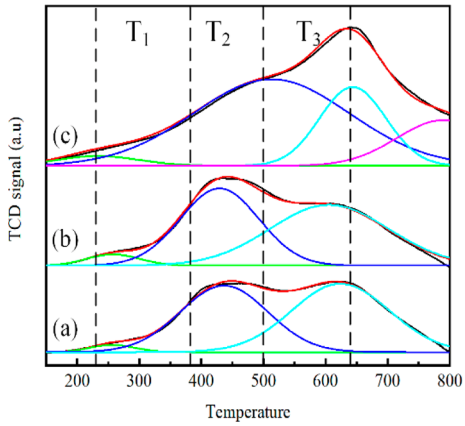

Figure 7. H_2-TPR profiles of Mn_3Ce_3/NAC catalysts: (a) before reaction; (b) after 150 °C reaction; (c) after 200 °C reaction.

to MnO would involve the presence of Mn_3O_4. However, after 200 °C reaction testing, the higher peak intensity at 644 °C pointed to relatively high concentrations of Ce^{4+}; also, for this sample, the broad, high-intensity reduction peak near 518 °C was due to the reduction of surface oxygen of ceria.[55]

2.3.5. C_2H_4-TPD/NO-TPD Analysis. The C_2H_4-TPD and NO-TPD data were shown in Figure 8. At 80−700 °C, Mn_3Ce_3/NAC catalysts had 3 desorption peaks for C_2H_4 and NO. In C_2H_4-TPD, the desorption peaks of the Mn_3Ce_3/NAC

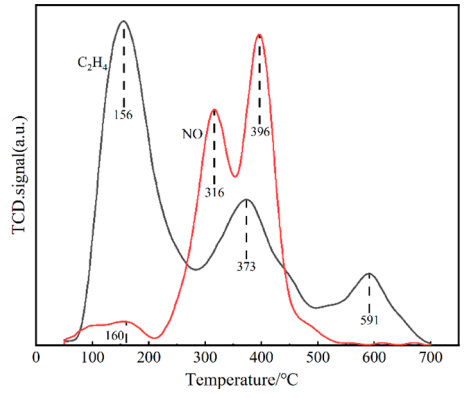

Figure 8. C_2H_4-TPD and NO-TPD of Mn_3Ce_3/NAC catalysts.

https://doi.org/10.1021/acsomega.2c00202
ACS Omega 2022, 7, 12004−12014

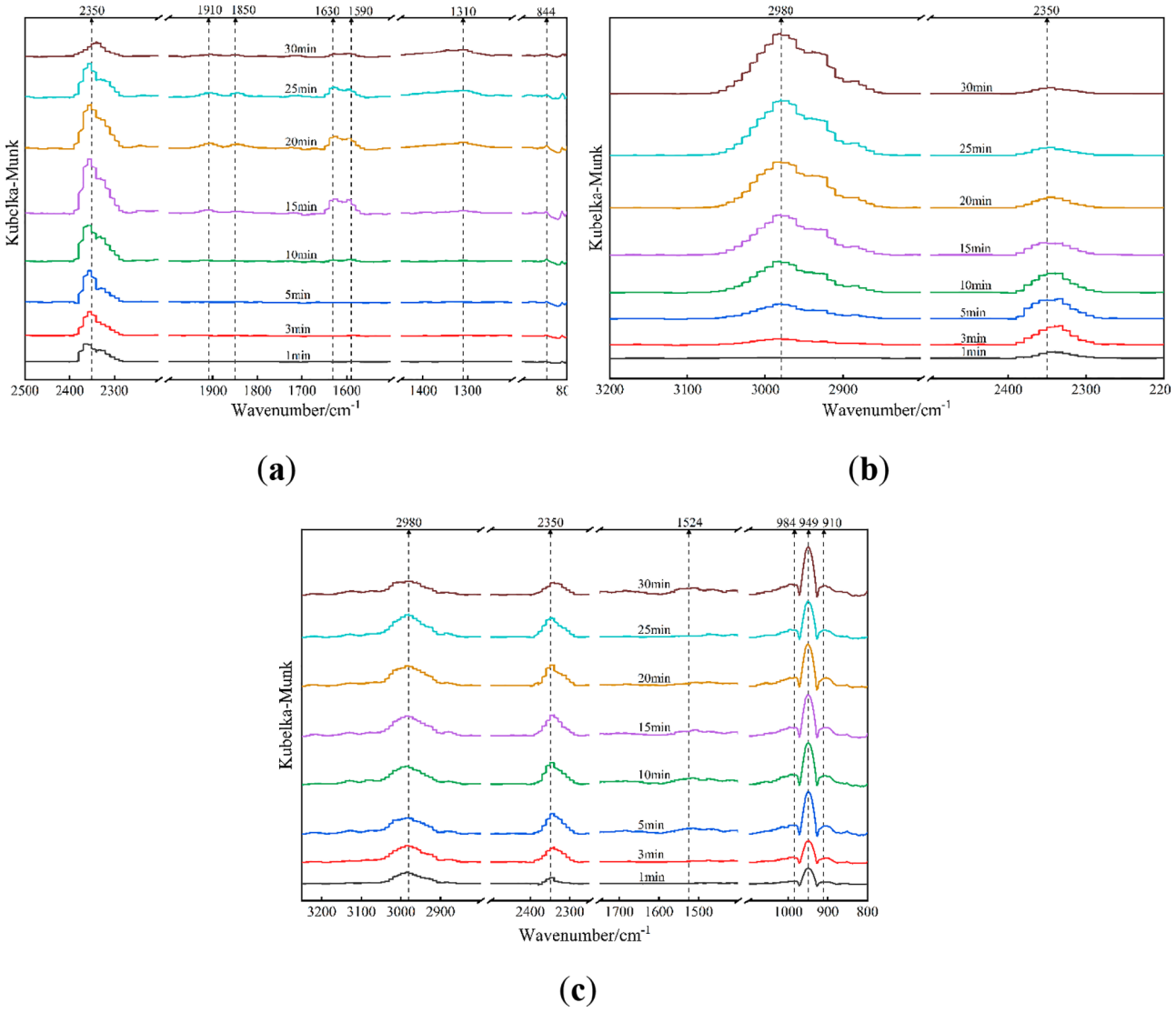

Figure 9. DRIFTS spectra of Mn_3Ce_3/NAC catalysts in a flow of (a) NO + O_2 + He; (b) C_2H_4 + O_2 + He; (c) C_2H_4 + NO + O_2 + He.

catalyst were located at 156, 373, and 591 °C. The 156 °C peak corresponded to the medium-strong acid site, and the peaks at 373 and 591 °C were attributed to the strong acid site. It can be seen from the C_2H_4-TPD spectrum that the distribution of medium-strong acid centers was greater than that of strong acid. The NO-TPD spectrum shows that the desorption peaks of the Mn_3Ce_3/NAC catalyst were distributed at 160, 316, and 396 °C. At 160 °C, the NO desorption peak was very small; that is, the corresponding medium-strong acid site content was relatively low, which indicated that under low temperature conditions, C_2H_4 was more easily adsorbed on the surface of Mn_3Ce_3/NAC catalyst.

2.3.6. In Situ DRIFTS Study. Figure 9a shows the DRIFTS spectra of Mn_3Ce_3/NAC catalysts in a flow condition of NO + O_2 + He at 200 °C. When the mixed gas was introduced for 1 min, a strong band appeared at 2350 cm^{-1}, which was attributed to CO_2.[56] Over time, other bands at 1910, 1850, 1630, 1590, 1310, and 844 cm^{-1} were detected. The peak at 1910 cm^{-1} corresponded to C−H; 1850 cm^{-1} peak was assigned to acid anhydride; 1630, 1590, and 1310 cm^{-1} were the characterization signals of NO_2^-;[57] and the band at 844 cm^{-1} was attributed to υ_sC−N. Therefore, nitrates on Mn_3Ce_3/NAC catalyst were formed from the reaction between NO and O_2.

Figure 9b shows the DRIFTS spectra of Mn_3Ce_3/NAC catalysts in a flow of C_2H_4 + O_2 + He at 200 °C. After the mixed gas was introduced, two strong absorption peaks appeared at 2350 and 2980 cm^{-1}, respectively; the peak at 2350 cm^{-1} was consistent with the band in Figure 10, which corresponds to CO_2, while the peak at 2980 cm^{-1} was attributed to the CH_2 and CH_3 stretching vibrations.[58]

Figure 9c shows the DRIFTS spectra of Mn_3Ce_3/NAC catalysts in a flow of C_2H_4 + NO + O_2 + He at 200 °C. At time of 1 min, there were 5 bands, and they were located at 2980, 2350, 984, 949, and 910 cm^{-1}, respectively. Among them, the peak at 2980 cm^{-1} was assigned to CH_2 and CH_3 stretching vibrations,[58] the band at 949 cm^{-1} was attributed to δO−H of R-COOH, the band at 2350 cm^{-1} was attributed to CO_2, the peak at 984 cm^{-1} was attributed σC−H of olefin, and the band at 910 cm^{-1} belongs to C−N. The band intensity at 1524 cm^{-1} was weak, and it belonged to $\upsilon_{as}COO^-$.[56]

Comparing Figure 9a−c, there was an absorption CO_2 peak under the three gas flow conditions, which may be the result of the oxygen-containing functional groups in the activated

https://doi.org/10.1021/acsomega.2c00202
ACS Omega 2022, 7, 12004−12014

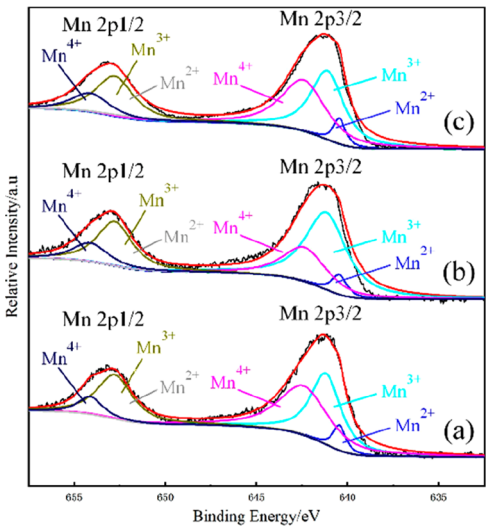

Figure 10. Deconvoluted XPS spectra of the Mn 2p: (a) before reaction; (b) after 150 °C reaction; (c) after 200 °C reaction.

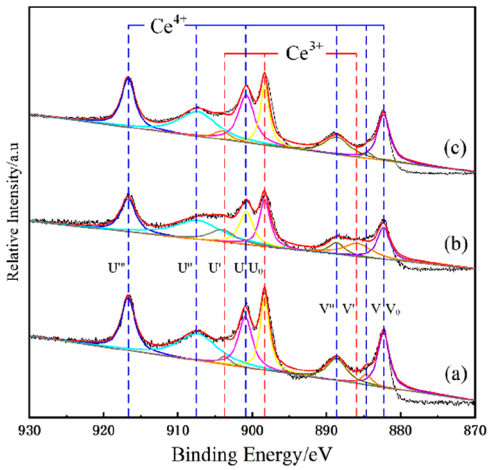

Figure 11. Deconvoluted XPS spectra of the Ce 3d: (a) before reaction; (b) after 150 °C reaction; (c) after 200 °C reaction.

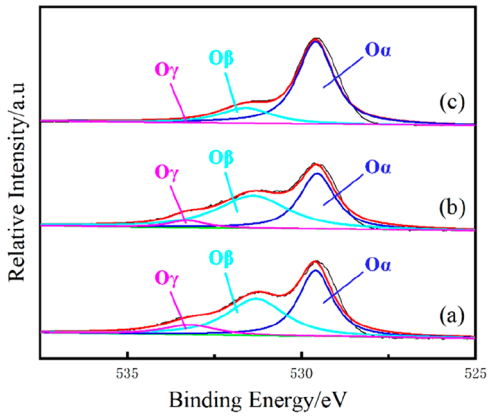

Figure 12. Deconvoluted XPS spectra of the O 1s: (a) before reaction; (b) after 150 °C reaction; (c) after 200 °C reaction.

carbon being oxidized by oxygen. From Figure 9a, it can be inferred that after the introduction of NO and O_2, NO was adsorbed on the surface of the Mn_3Ce_3/NAC in situ catalyst and generated nitrate. Figure 9b shows that ethylene had a good adsorption capacity on the Mn_3Ce_3/NAC catalyst and produced the important intermediate products in the HC-SCR, which can be partially oxidized to generate hydrocarbon activated intermediates. Figure 9c demonstrated that when C_2H_4 + NO + O_2 was introduced, strong peaks R-COOH and weak peak of unidentate nitrate appeared, which indicated that ethylene was more easily adsorbed on the catalyst surface.

Based on the above results, during the HC-SCR reaction, the C_2H_4−SCR reaction route was determined as the ethylene being first adsorbed on Mn_3Ce_3/NAC catalysts to produce the intermediate products containing CH_2 or CH_3, and then reacted with NO to further produce products containing R-COOH, nitro, and C−N, and finally decomposed into final products H_2O, CO_2, and N_2, which indicated that the C_2H_4−SCR reaction following the E-R mechanism.[59−61]

2.3.7. Binding State of Constituent Elements. Oxidation states of catalytically active species worked as an essential role in the catalytic performance;[62] hence, XPS analyses of the Mn_3Ce_3/NAC catalysts were also performed, the data from which are presented in Figures 10, 11, and 12. As shown in Figure 10, the main peaks of Mn $2p_{3/2}$ deconvoluted into contributions from respective oxidation states, including 642.4, 641.2, and 640.5 eV corresponding to Mn^{4+}, Mn^{3+}, and Mn^{2+}, respectively.[63] Similarly, the peaks at 654.1, 652.8, and 651.1 eV were ascribed to Mn^{4+}, Mn^{3+}, and Mn^{2+} for Mn $2p_{1/2}$, respectively.[63] In addition to contributions to peak intensities from the three oxidation states of Mn, the intensity ratios of $Mn^{4+}/(Mn^{2+} + Mn^{3+} + Mn^{4+})$ and $Mn^{2+}/(Mn^{2+} + Mn^{3+} + Mn^{4+})$—labeled as Mn^{4+}/Mn^{n+} and Mn^{2+}/Mn^{n+} ratios in Table 2—are presented in Table 2. The catalyst before and after it was tested at 200 °C had high Mn^{4+}/Mn^{n+} ratios near 41%, whereas this ratio was 30% after 150 °C reaction testing. Hence, the contribution of Mn^{4+} was significantly less in the catalyst tested at 150 °C; it matched the XRD results in which the intensity of peaks for the catalyst after the reaction at 150 °C decreased.

Table 2. Chemical States and the Ratios of Relative Concentrations of Mn, Ce, and O for Different Catalysts

samples	Mn^{4+}/Mn^{n+} (%)	Mn^{2+}/Mn^{n+} (%)	$Ce^{4+}/(Ce^{4+} + Ce^{3+})$ (%)	Oα (%)	Oβ (%)	Oγ (%)
Before reaction	41.5	4.7	79.8	46.0	43.5	10.5
After 150 °C reaction	30.0	4.5	67.3	50.9	43.8	5.3
After 200 °C reaction	40.9	6.9	81.8	79.0	20.9	0.1

Relative to the contribution of Mn^{4+} to HC-SCR, it is known that the activity of MnO_x species follows the order of MnO_2 > Mn_5O_8 > Mn_2O_3 > Mn_3O_4 > MnO,[64] suggesting that the existence of high oxidation state Mn was favorable for NO conversion. Furthermore, the acceleration effect of Mn^{4+} to the oxidation of NO to NO_2 has been attested, which could then impact SCR reactions through a "fast SCR" pathway.[65] Less Mn^{4+} in the catalyst tested at 150 °C was also suggested by the H_2-TPR data.

As shown in Figure 11, the Ce 3d spectra of the fresh and tested catalyst samples were split into nine main peaks. There are four pairs of spin−orbit doublets, and the nine peaks at 882.3, 884.6, 885.8, 888.6, 898.3, 900.8, 904, 907.3, and 916.7 eV were respectively marked as V_0, V, V′, V″, U_0, U, U′, U″,

https://doi.org/10.1021/acsomega.2c00202
ACS Omega 2022, 7, 12004−12014

and U‴. Due to the spin−orbit of the Ce $3d_{5/2}$ and Ce $3d_{3/2}$, the peaks were labeled V and U, respectively.[66,67] The V_0, V, V″, U, U″, and U‴ peaks were associated with the Ce^{4+}, while the peaks denoted as U_0, U′, and V′ corresponded to the Ce^{3+} species. Hence, the coexistence of Ce^{3+} and Ce^{4+} in Mn_3Ce_3/NAC was confirmed through the Ce 3d XPS spectra. It was discovered that the coexisting ion pair Ce^{3+}/Ce^{4+} species could create a charge imbalance, unsaturated chemical bonds, and oxygen vacancies on surfaces; these were in favor of the formation of chemisorbed oxygen during reaction testing.[68]

As shown in Table 2, the ratio of $[Ce^{4+}/(Ce^{4+} + Ce^{3+})]$ in the fresh catalyst and after 200 °C reaction testing was about 80%. According to the literature,[69] the incorporation of Ce in Mn compounds can create a Mn−O−Ce bridge during CeO_2 formation that also strengthens the bond between Mn and oxygen and promotes the valence of Mn from Mn^{3+} to Mn^{4+} through $Mn_2O_3 + 2CeO_2 \rightarrow 2MnO_2 + Ce_2O_3$. Hence, the existence of an oxygen vacancy and facile Ce^{3+}/Ce^{4+} couple could prevent the reduction of MnO_2 to Mn_2O_3 while simultaneously creating larger Ce^{4+} concentrations through the redox cycle of $Mn^{3+} + Ce^{4+} \leftrightarrow Mn^{4+} + Ce^{3+}$.[66] Then, the presence of a stable Mn^{4+} is suggested to facilitate HC-SCR reactions. In other words, the 79% and 81% Ce^{4+} ratios on the fresh and 200 °C reaction tested samples, and the stable NO conversion, are in accordance with this interpretation.

Figure 12 describes the XPS spectra for O 1s of the catalysts in which the deconvolution of the peaks was accomplished using three peaks. The binding energies of peaks were approximately 529.6, 531.1, and 533.2 eV, credited to lattice oxygen (O^{2-}, marked as O_α), surface chemical oxygen (O_2^{2-} or O^-, marked as O_β), and the oxygen species in hydroxide groups which was marked as O_γ, respectively.[66] The relative intensity of O_β changed intensely after the HC-SCR reactions. Thus, the surface chemisorbed oxygen has also been more correlated to higher catalytic activity than lattice oxygen as a result of its higher mobility.[69] As shown in Table 2, the ratios of O_β were greater than for most other catalysts,[70] the ratio of $O_\beta/(O_\alpha + O_\beta)$ on the Mn_3Ce_3/NAC catalysts before reaction, after 150 °C reaction, and after 200 °C reaction are 0.49, 0.46, and 0.21; for the SCR reaction, the high ratio of $O_\beta/(O_\alpha + O_\beta)$ means that NO is more easily oxidized to NO_2, which is an important intermediate to generate N_2, and suggests ample presence of facile oxygen for catalytic reactivity.

Therefore, the analytical characterization data of Mn_3Ce_3/NAC catalysts before and after the reaction testing point to a reaction sequence during HC-SCR as depicted in Figure 13. The presence of CeO_2 in a sufficient concentration is critical for stable NO conversion, because it helps to prevent the reduction of MnO_2 to Mn_2O_3 by promoting the forward reaction and simultaneously, through synergistic interactions, promotes the establishment of relatively high concentrations of facile, absorbed oxygen on the catalyst surface. Therefore, C_2H_4 is more easily oxidized to produce the hydrocarbon activated intermediate, −COOH, which promotes the C_2H_4−SCR reaction. When the CeO_2 concentrations were not high enough or the reaction temperature was too low, a precipitous decrease in NO activity occurred immediately after reaction testing had begun, because the Ce species were agglomerated into small, isolated CeO_2 crystallites which did not effectively interact with the MnO_x and did not mitigate the formation of low-activity Mn_3O_4 species.

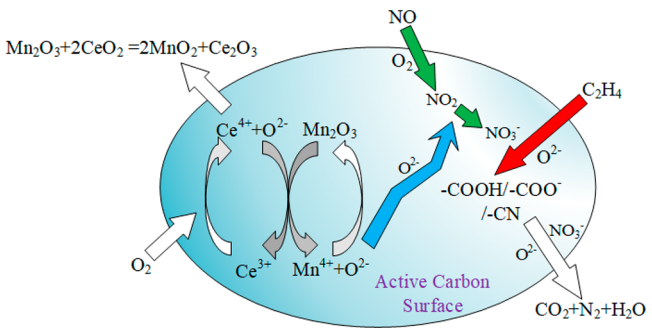

Figure 13. Synergistic mechanism for HC-SCR of NO on Mn_3Ce_3/NAC catalysts.

3. EXPERIMENTAL METHODS

3.1. Catalyst Preparation. Active carbon used was purchased from MACKLIN with particle size range of 1000−2350 μm. The raw AC was first treated with 10% HNO_3 solution for 4 h under room temperature and washed with deionized water until the pH of the wastewater became neutral, and finally the AC was dried under air atmosphere at 140 °C for 14 h. These HNO_3-treated AC supports were named as NAC.

The Mn−Ce/AC catalysts with MnO_2 and CeO_2 loadings were prepared by impregnation of the NAC using $Mn(NO_3)_2 \cdot 4H_2O$ and $Ce(NO_3)_3 \cdot 6H_2O$ solutions to attain a Mn loading of about 3.0 wt % and Ce loadings of 3.0, 5.0, and 7.0 wt %; sonication of these mixtures was at room temperature for 2 h. Then, the hybrids stand for 12 h, after which they were filtered and dried in a vacuum oven heated to 110 °C, and finally calcined at 400 °C for 2 h in a hermetic muffle furnace under N_2 atmosphere. The synthesized materials were labeled as Mn_3Ce_x/NAC, where X = 3, 5, 7.

3.2. Catalyst Characterization. The synthesized materials were characterized analytically before and after reaction testing. After degassing overnight at 160 °C and isothermal N_2 adsorption−desorption measurements taken at 77 K, surface area and porosity were measured in a Micromeritics ASAP 2020 analyzer.

Crystalline structures were performed by X-ray diffraction (XRD) using Cu Kα irradiation with a 2θ range of 90°. The microstructure was examined by scanning electron microscope (SEM) with energy-dispersive X-ray spectroscopy (EDS). X-ray photoelectron spectroscopy (XPS) was performed on a Thermo Fisher ESCALAB 250Xi instrument, and the data were calibrated using the ubiquitous C 1s peak at 284.8 eV.

The temperature-programmed reduction (TPR) data were acquired using an AutoChem II 2920 instrument; approximately 0.1 g samples were placed in a U-shaped quartz tube which was then pretreated in O_2 flow at 300 °C for 1 h. After the samples were cooled to room temperature, 5% H_2 in helium was flowed through the tube at a flow rate of 30 mL/min while the temperature was increased from room temperature to 900 °C at a rate of 10 °C/min.

The temperature-programmed desorption (TPD) study was performed on an AutoChem II 2920 instrument: 0.1 g sample was pretreated in helium at 300 °C for 1 h; afterward the sample was cooled to room temperature, and C_2H_4 or NO in helium was purged to the tube at a flow rate of 30 mL/min as the temperature was increased from 80 to 700 °C at a rate of 10 °C/min.

https://doi.org/10.1021/acsomega.2c00202
ACS Omega 2022, 7, 12004−12014

In situ DRIFTS was performed on a VERTEX 80 V instrument: 0.2 g sample was pretreated in helium at 200 °C for 30 min, and signals were collected as the background spectrum. Then, the NO + O_2, C_2H_4 + O_2, and C_2H_4 + NO + O_2 was separately flowed into the reactor at 30 mL/min, and the sample spectra at 1, 3, 5, 10, 15, 20, 25, and 30 min were collected (scanning times, 128; resolution, 4 cm^{-1}, scanning range, 4000−600 cm^{-1}).

3.3. Catalytic Activity Testing. The activity evaluation equipment of the prepared catalysts (Figure 14) involved a

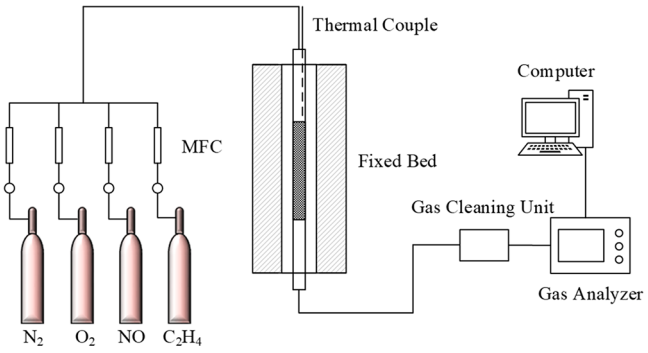

Figure 14. Schematic of the bench-scale setup.

fixed bed, a gas analyzer (MRU MGA5), a gas cleaning unit, several mass flow controllers (MFCs, MF SHY 400), and a quartz tube reactor (I.D. = 10 mm) heated by a temperature-controlled furnace; the initial weight of a sample for each test was 10 g. Total gas flow at a rate of 1500 mL/min was controlled by mass flow controllers (MFCs, MF SHY 400). The components of the simulated flue gas were 500 ppm of NO, 250 ppm of C_2H_4, 3 vol % O_2, and N_2 as a balance. The catalyst sample was in N_2 atmosphere during the heating procedure; once the temperature remained unchanged, the mixture was flowed into the reactor, and then NO and NO_x gas concentrations at the outlet of the reactor were analyzed using a flue gas analyzer (MRU). From these concentration data, NO conversion and N_2 selectivity data were calculated through the following equation:

$$\text{NO conversion}(\%) = \left(1 - \frac{[NO]_{out}}{[NO]_{in}}\right) \times 100 \quad (2)$$

$$N_2 \text{ selectivity}(\%) = \left(1 - \frac{[NO_2]_{out} + 2 \times [N_2O]_{out}}{[NO]_{in} - [NO]_{out}}\right) \times 100 \quad (3)$$

4. CONCLUSIONS

This study focused on examining the potential development of stable and active Mn_3Ce_x/NAC catalysts used for HC-SCR with C_2H_4 as a reductant and on understanding catalyst physical and chemical properties important for NO conversion with temperatures at or below 200 °C. The catalysts were prepared, tested for HC-SCR catalytic activity, and analyzed before and after reaction testing using surface sensitive and bulk techniques. The conclusions include the following:

1. The addition of CeO_2 to the MnO_x established stable and high HC-SCR catalytic performance when the reaction temperature was at least 200 °C and the CeO_x/MnO_x concentration ratio was 1 or reaction temperature was below 200 °C and the CeO_x/MnO_x concentration ratio was > 1.
2. The reaction mechanism followed the E-R mechanism, and ethylene was first adsorbed on the Mn_3Ce_3/NAC catalysts to produce the intermediate products containing CH_2 or CH_3, which can be partially oxidized to generate hydrocarbon activated intermediate, R-COOH.
3. Stable activity was proposed to be a result of the formation of CeO_2 at a sufficient concentration that could prevent the reduction of Mn^{4+} and, simultaneously, the creation of Ce^{3+}/Ce^{4+} redox couples that would help to reoxidize any reduced Mn.
4. The addition of CeO_2 promoted the formation of Mn−O−Ce bridges with MnO_x that then helped to enhance the concentration of surface chemisorbed oxygen and oxygen vacancies. This study provided new and intriguing insight into approaches to instill effective catalytic activity into transition metal oxide catalysts for low-temperature HC-SCR applications.

AUTHOR INFORMATION

Corresponding Author

Fang Liu − *School Of Low-Carbon Energy And Power Engineering, China University of Mining and Technology, Xuzhou 221116 Jiangsu, China*; orcid.org/0000-0003-1001-3924; Email: fang.liu@cumt.edu.cn

Authors

Jiangyuan Zhao − *School Of Low-Carbon Energy And Power Engineering, China University of Mining and Technology, Xuzhou 221116 Jiangsu, China*

Shengbao He − *Petrochemical Research Institute of PetroChina, Beijing 102206, China*

Qing Liu − *School Of Low-Carbon Energy And Power Engineering, China University of Mining and Technology, Xuzhou 221116 Jiangsu, China*

Guangli Liu − *Lanzhou Petrochemical Research Center, PetroChina, Lanzhou 730060 Gansu, China*

Li Yang − *School Of Low-Carbon Energy And Power Engineering, China University of Mining and Technology, Xuzhou 221116 Jiangsu, China*

Complete contact information is available at: https://pubs.acs.org/10.1021/acsomega.2c00202

Author Contributions

Fang Liu: Formal analysis, Data curation, Methodology, Visualization, Writing − original draft. Jiangyuan Zhao: Methodology, Investigation, Validation, Writing − original draft, Writing − review and editing. Shengbao He: Formal analysis, Writing − review and editing. Qing Liu: Project administration, Writing − review and editing. Guangli Liu: Validation, Writing − review and editing. Li Yang: Supervision, Writing − review and editing.

Notes

The authors declare no competing financial interest.

ACKNOWLEDGMENTS

This work was supported by "the Fundamental Research Funds for the Central Universities" with the contract No. 2019XKQYMS39.

https://doi.org/10.1021/acsomega.2c00202
ACS Omega 2022, 7, 12004−12014

REFERENCES

(1) Gunnarsson, F.; Granlund, M. Z.; Englund, M.; Dawody, J.; Pettersson, L. J.; Härelind, H. Combining HC-SCR over Ag/Al2O3 and hydrogen generation over Rh/CeO2-ZrO2 using biofuels: An integrated system approach for real applications. *Appl. Catal., B* **2015**, *162*, 583−592.

(2) Nguyen, D. B.; Nguyen, V. T.; Heo, I. J.; Mok, Y. S. Removal of NOx by selective catalytic reduction coupled with plasma under temperature fluctuation condition. *J. Ind. Eng. Chem.* **2019**, *72*, 400−407.

(3) Wang, Y.; Kapteijn, F.; Makkee, M. NOx reduction in the Di-Air system over noble metal promoted ceria. *Appl. Catal., B* **2018**, *231*, 200−212.

(4) Van Caneghem, J.; De Greef, J.; Block, C.; Vandecasteele, C. NOx reduction in waste incinerators by selective catalytic reduction (SCR) instead of selective non catalytic reduction (SNCR) compared from a life cycle perspective: a case study. *J. Cleaner Prod* **2016**, *112*, 4452−4460.

(5) Prieto-Centurion, D.; Eaton, T. R.; Roberts, C. A.; Fanson, P. T.; Notestein, J. M. Catalytic reduction of NO with H2 over redox-cycling Fe on CeO2. *Appl. Catal., B* **2015**, *168−169*, 68−76.

(6) Chen, C.; Cao, Y.; Liu, S.; Chen, J.; Jia, W. Review on the latest developments in modified vanadium-titanium-based SCR catalysts. *Chin. J. Catal* **2018**, *39* (8), 1347−1365.

(7) Zhao, Q.; Chen, B.; Bai, Z.; Yu, L.; Crocker, M.; Shi, C. Hybrid catalysts with enhanced C3H6 resistance for NH3-SCR of NOx. *Appl. Catal., B* **2019**, *242*, 161−170.

(8) Busca, G.; Lietti, L.; Ramis, G.; Berti, F. Chemical and mechanistic aspects of the selective catalytic reduction of NOx by ammonia over oxide catalysts: A review. *Appl. Catal., B* **1998**, *18* (1), 1−36.

(9) Yu, J.; Li, C.; Guo, F.; Gao, S.; Zhang, Z.; Matsuoka, K.; Xu, G. The pilot demonstration of a honeycomb catalyst for the DeNOx of low-temperature flue gas from an industrial coking plant. *Fuel* **2018**, *219*, 37−49.

(10) Hansen, K. K. Solid state electrochemical DeNOx—An overview. *Appl. Catal., B* **2010**, *100* (3), 427−432.

(11) Huang, N.; Geng, Y.; Xiong, S.; Huang, X.; Kong, L.; Yang, S.; Peng, Y.; Chen, J.; Li, J. The promotion effect of ceria on high vanadia loading NH3-SCR catalysts. *Catal. Commun.* **2019**, *121*, 84−88.

(12) Cha, W.; Ehrman, S. H.; Jurng, J. CeO2 added V2O5/TiO2 catalyst prepared by chemical vapor condensation (CVC) and impregnation method for enhanced NH3-SCR of NOx at low temperature. *J. Environ. Chem. Eng.* **2016**, *4* (1), 556−563.

(13) Liu, Z.; Zhang, S.; Li, J.; Zhu, J.; Ma, L. Novel V2O5-CeO2/TiO2 catalyst with low vanadium loading for the selective catalytic reduction of NOx by NH3. *Appl. Catal., B* **2014**, *158−159*, 11−19.

(14) Castellanos, I.; Marie, O. An operando FT-IR study of the NOx SCR over Co-HFER and Fe-HFER using acetylene as a reducing agent. *Catal. Today* **2017**, *283*, 54−65.

(15) Colombo, M.; Nova, I.; Tronconi, E. A simplified approach to modeling of dual-layer ammonia slip catalysts. *Chem. Eng. Sci.* **2012**, *75*, 75−83.

(16) Chen, W.; Ma, Y.; Yan, N.; Qu, Z.; Yang, S.; Xie, J.; Guo, Y.; Hu, L.; Jia, J. The co-benefit of elemental mercury oxidation and slip ammonia abatement with SCR-Plus catalysts. *Fuel* **2014**, *133*, 263−269.

(17) Chen, W.; Qu, Z.; Huang, W.; Hu, X.; Yan, N. Novel effect of SO2 on selective catalytic oxidation of slip ammonia from coal-fired flue gas over IrO2 modified Ce-Zr solid solution and the mechanism investigation. *Fuel* **2016**, *166*, 179−187.

(18) Liu, L.; Wang, L.; Su, S.; Yang, T.; Dai, Z.; Qing, M.; Xu, K.; Hu, S.; Wang, Y.; Xiang, J. Leaching behavior of vanadium from spent SCR catalyst and its immobilization in cement-based solidification/stabilization with sulfurizing agent. *Fuel* **2019**, *243*, 406−412.

(19) Rajendran, N.; Seagrave, J. C.; Plunkett, L. M.; MacGregor, J. A. A comparative assessment of the acute inhalation toxicity of vanadium compounds. *Inhal. Toxicol* **2016**, *28* (13), 618−628.

(20) Yang, L.; Jia, Y.; Cheng, J.; Wu, X.; He, J.; Liu, F. Deactivation mechanism of activated carbon supported copper oxide SCR catalysts in C2H4 reductant. *Canadian Journal of Chemical Engineering* **2019**, *97*, 2708−2716.

(21) Yan, Q.; Chen, S.; Zhang, C.; Wang, Q.; Louis, B. Synthesis and catalytic performance of Cu1Mn0.5Ti0.5Ox mixed oxide as low-temperature NH3-SCR catalyst with enhanced SO2 resistance. *Appl. Catal., B* **2018**, *238*, 236−247.

(22) Niu, Y.; Shang, T.; Hui, S.; Zhang, X.; Lei, Y.; Lv, Y.; Wang, S. Synergistic removal of NO and N2O in low-temperature SCR process with MnOx/Ti based catalyst doped with Ce and V. *Fuel* **2016**, *185*, 316−322.

(23) Zhang, G.; Han, W.; Zhao, H.; Zong, L.; Tang, Z. Solvothermal, synthesis of well-designed ceria-tin-titanium catalysts with enhanced catalytic performance for wide temperature NH3-SCR reaction. *Appl. Catal., B* **2018**, *226*, 117−126.

(24) Männikkö, M.; Skoglundh, M.; Ingelsten, H. H. Selective catalytic reduction of NOx with methanol over supported silver catalysts. *Appl. Catal., B* **2012**, *119−120*, 256−266.

(25) Gao, F.; Tang, X.; Yi, H.; Zhao, S.; Wang, J.; Gu, T. Improvement of activity, selectivity and H2O&SO2-tolerance of micro-mesoporous CrMn2O4 spinel catalyst for low-temperature NH3-SCR of NOx. *Appl. Surf. Sci.* **2019**, *466*, 411−424.

(26) Kowalczyk, A.; Święs, A.; Gil, B.; Rutkowska, M.; Piwowarska, Z.; Borcuch, A.; Michalik, M.; Chmielarz, L. Effective catalysts for the low-temperature NH3-SCR process based on MCM-41 modified with copper by template ion-exchange (TIE) method. *Appl. Catal., B* **2018**, *237*, 927−937.

(27) Arfaoui, J.; Ghorbel, A.; Petitto, C.; Delahay, G. Novel V2O5-CeO2-TiO2-SO42- nanostructured aerogel catalyst for the low temperature selective catalytic reduction of NO by NH3 in excess O2. *Appl. Catal., B* **2018**, *224*, 264−275.

(28) More, P. M.; Nguyen, D. L.; Granger, P.; Dujardin, C.; Dongare, M. K.; Umbarkar, S. B. Activation by pretreatment of Ag-Au/Al2O3 bimetallic catalyst to improve low temperature HC-SCR of NOx for lean burn engine exhaust. *Appl. Catal., B* **2015**, *174−175*, 145−156.

(29) Wang, X.; Chen, H.; Sachtler, W. M. H. Selective reduction of NOx with hydrocarbons over Co/MFI prepared by sublimation of CoBr2 and other methods. *Appl. Catal., B* **2001**, *29* (1), 47−60.

(30) Dzwigaj, S.; Janas, J.; Gurgul, J.; Socha, R. P.; Shishido, T.; Che, M. Do Cu(II) ions need Al atoms in their environment to make CuSiBEA active in the SCR of NO by ethanol or propane? A spectroscopy and catalysis study. *Appl. Catal., B* **2009**, *85* (3), 131−138.

(31) Houel, V.; James, D.; Millington, P.; Pollington, S.; Poulston, S.; Rajaram, R.; Torbati, R. A comparison of the activity and deactivation of Ag/Al2O3 and Cu/ZSM-5 for HC-SCR under simulated diesel exhaust emission conditions. *J. Catal.* **2005**, *230* (1), 150−157.

(32) Nam, K. B.; Kim, D. H.; Hong, S. C. Enhancement of Mn/Ce/W/Ti catalysts through control of pH and oxygen mobility during their preparation. *Appl. Catal., A* **2019**, *572*, 107−114.

(33) Xu, G.; Ma, J.; Wang, L.; Xie, W.; Liu, J.; Yu, Y.; He, H. Insight into the origin of sulfur tolerance of Ag/Al2O3 in the H2-C3H6-SCR of NOx. *Appl. Catal., B* **2019**, *244*, 909−918.

(34) Peña, D. A.; Uphade, B. S.; Smirniotis, P. G. TiO2-supported metal oxide catalysts for low-temperature selective catalytic reduction of NO with NH3: I. Evaluation and characterization of first row transition metals. *J. Catal.* **2004**, *221* (2), 421−431.

(35) Qiu, L.; Wang, Y.; Pang, D.; Ouyang, F.; Zhang, C. SO_4^{2-}-Mn-Co-Ce supported on TiO2/SiO2 with high sulfur durability for low-temperature SCR of NO with NH3. *Catal. Commun.* **2016**, *78*, 22−25.

(36) Wang, X.; Zheng, Y.; Lin, J. Highly dispersed Mn-Ce mixed oxides supported on carbon nanotubes for low-temperature NO reduction with NH3. *Catal. Commun.* **2013**, *37* (13), 96−99.

(37) Liu, F.; Xuan, G.; Ai, L.; Liu, Q.; Yang, L. Key factors that affect catalytic activity of activated carbon-based catalyst in chemical

https://doi.org/10.1021/acsomega.2c00202
ACS Omega 2022, 7, 12004−12014

looping methane decomposition for H2 production. *Fuel Process. Technol.* **2021**, *215*, 106745.
(38) Xuan, G.; Liu, F.; Zhang, F.; Hu, Y.; Miao, J.; Yang, Li. Mechanism of improving the stability of activated carbon catalyst by trace H2S impurities in natural gas for hydrogen production from methane decomposition. *Fuel* **2021**, *299* (2021), 120884.
(39) Tang, X.; Hao, J.; Yi, H.; Li, J. Low-temperature SCR of NO with NH3 over AC/C supported manganese-based monolithic catalysts. *Catal. Today* **2007**, *126* (3), 406−411.
(40) Liu, G.; Han, D.; Cheng, J.; Feng, Y.; Quan, W.; Yang, L.; Saito, K. Performance of C2H4 Reductant in Activated-Carbon- Supported MnOx-based SCR Catalyst at Low Temperatures. *Energies* **2019**, *12* (1), 123.
(41) Liu, F.; Chen, L.; Neathery, J. K.; Saito, K.; Liu, K. Cerium Oxide Promoted Iron-based Oxygen Carrier for Chemical Looping Combustion. *Ind. Eng. Chem. Res.* **2014**, *53* (42), 16341−16348.
(42) Qi, G.; Yang, R. T.; Chang, R. MnOx-CeO2 mixed oxides prepared by co-precipitation for selective catalytic reduction of NO with NH3 at low temperatures. Applied Catalysis B. *Environmental* **2004**, *51* (2), 93−106.
(43) Liu, Z.; Yi, Y.; Zhang, S.; Zhu, T.; Zhu, J.; Wang, J. Selective catalytic reduction of NOx with NH3 over Mn-Ce mixed oxide catalyst at low temperatures. *Catal. Today* **2013**, *216*, 76−81.
(44) Boningari, T.; Ettireddy, P. R.; Somogyvari, A.; Liu, Y.; Vorontsov, A.; McDonald, C. A.; Smirniotis, P. G. Influence of elevated surface texture hydrated titania on Ce-doped Mn/TiO2 catalysts for the low-temperature SCR of NOx under oxygen-rich conditions. *J. Catal.* **2015**, *325*, 145−155.
(45) Andersen, N. I.; Serov, A.; Atanassov, P. Metal oxides/CNT nano-composite catalysts for oxygen reduction/oxygen evolution in alkaline media. *Appl. Catal., B* **2015**, *163*, 623−627.
(46) LI, L.; WU, Y.; Hou, X.; Chu, B.; Nan, B.; Qin, Q.; Fan, M.; Sun, C.; Li, B.; Dong, L.; Dong, L. Investigation of Two-Phase Intergrowth and Coexistence in Mn-Ce-Ti-O Catalysts for the Selective Catalytic Reduction of NO with NH3: Structure-Activity Relationship and Reaction Mechanism[J]. *Ind. Eng. Chem. Res.* **2019**, *58* (2), 849−862.
(47) Meng, L.; Wang, J.; Sun, Z.; Zhu, J.; Li, H.; Wang, J.; Shen, M. Active Manganese Oxide On MnOx-CeO2 Catalysts for Low-Temperature NO Oxidation: Characterization and Kinetics Study. *J. Rare Earths* **2018**, *36*, 142−147.
(48) Oberlin, A. Carbonization and graphitization. *Carbon* **1984**, *22* (6), 521−541.
(49) Wang, X.; Zheng, Y.; Lin, J. Highly dispersed Mn-Ce mixed oxides supported on carbon nanotubes for low-temperature NO reduction with NH3. *Catal. Commun.* **2013**, *37* (13), 96−99.
(50) France, L. J.; Yang, Q.; Li, W.; Chen, Z.; Guang, J.; Guo, D.; Wang, L.; Li, X. Ceria modified FeMnOx—Enhanced performance and sulphur resistance for low-temperature SCR of NOx. *Appl. Catal., B* **2017**, *206*, 203−215.
(51) Yang, J.; Ren, S.; Zhang, T.; Su, Z.; Long, H.; Kong, M.; Yao, L. Iron doped effects on active sites formation over activated carbon supported Mn-Ce oxide catalysts for low-temperature SCR of NO. *Chem. Eng. J.* **2020**, *379*, 122398.
(52) Gu, X.; Ge, J.; Zhang, H.; Auroux, A.; Shen, J. Structural, redox and acid-base properties of V2O5/CeO2 catalysts. *Thermochim. Acta* **2006**, *451* (1), 84−93.
(53) Kapteijn, F.; Singoredjo, L.; Andreini, A.; Moulijn, J. A. Activity and selectivity of pure manganese oxides in the selective catalytic reduction of nitric oxide with ammonia. *Appl. Catal., B* **1994**, *3* (2−3), 173−189.
(54) Huang, J.; Huang, H.; Jiang, H.; Liu, L. The promotional role of Nd on Mn/TiO2 catalyst for the low-temperature NH3-SCR of NOx. *Catal. Today* **2019**, *332*, 49.
(55) Zhou, L.; Li, C.; Zhao, L.; Zeng, G.; Gao, L.; Wang, Y.; Yu, M. The poisoning effect of PbO on Mn-Ce/TiO2 catalyst for selective catalytic reduction of NO with NH3 at low temperature. *Appl. Surf. Sci.* **2016**, *389*, 532−539.
(56) Halkides, T. I.; Kondarides, D. I.; Verykios, X. E. Mechanistic study of the reduction of NO by C3H6 in the presence of oxygen over Rh/TiO2 catalysts. *Catal. Today* **2002**, *73*, 213−221.
(57) Chen, H.; Voskoboinikov, T.; Sachtler, W. M. H. Reduction of NOx over Fe/ZSM-5 Catalysts: Adsorption Complexes and Their Reactivity toward Hydrocarbons. *J. Catal.* **1998**, *180*, 171−183.
(58) Jiang, J.; Pan, H.; Sun, G.; Ye, Q.; Shao, Z.; Shi, Y. Promotion of Ni/H-BEA by Fe for NOx Reduction with Propane in a Lean-Burn Condition. *Energy Fuels* **2011**, *25*, 4377−4383.
(59) He, L.; Ma, X.; Cui, S.; Wan, Y. The Adsorption Behavior and Reaction Mechanism of MnOx/TiO2 Catalytic Materials to NO and NH3 by DRIFTS [J]. *Materials Report* **2018**, *32* (22), 3973−3978.
(60) Liu, Z.; Feng, X.; Zhou, Z.; Feng, Y.; Li, J. Ce-sn binary oxide catalyst for the selective catalytic reduction of nox by nh3. *Appl. Surf. Sci.* **2018**, *428*, 526−33.
(61) Yang, S.; Qi, F.; Xiong, S.; Dang, H.; Liao, Y.; Wong, P. K.; Li, J. MnOx supported on fe-ti spinel: a novel mn based low temperature scr catalyst with a high n2 selectivity. *Applied Catalysis B: Environmental* **2016**, *181*, 570−80.
(62) Kwon, D. W.; Nam, K. B.; Hong, S. C. Influence of tungsten on the activity of a Mn/Ce/W/Ti catalyst for the selective catalytic reduction of NO with NH3 at low temperatures. *Appl. Catal., A* **2015**, *497*, 160−166.
(63) Chen, S.; Yan, Q.; Zhang, C.; Wang, Q. A novel highly active and sulfur resistant catalyst from Mn-Fe-Al layered double hydroxide for low temperature NH3-SCR. *Catal. Today* **2019**, *327*, 81−89.
(64) Sultana, A.; Sasaki, M.; Hamada, H. Influence of support on the activity of Mn supported catalysts for SCR of NO with ammonia. *Catal. Today* **2012**, *185* (1), 284−289.
(65) Zhang, L.; Zhang, D.; Zhang, J.; Cai, S.; Fang, C.; Huang, L.; Li, H.; Gao, R.; Shi, L. Design of meso-TiO2@MnOx-CeOx/CNTs with a core-shell structure as DeNOx catalysts: promotion of activity, stability and SO2-tolerance. *Nanoscale* **2013**, *5* (20), 9821−9829.
(66) Jiang, L.; Liu, Q.; Ran, G.; Kong, M.; Ren, S.; Yang, J.; Li, J. V2O5-modified Mn-Ce/AC catalyst with high SO2 tolerance for low-temperature NH3-SCR of NO. *Chem. Eng. J.* **2019**, *370*, 810−821.
(67) Rocha, M.A. L.; Del Angel, G.; Torres-Torres, G.; Cervantes, A.; Vazquez, A.; Arrieta, A.; Beltramini, J.N. Effect of the Pt oxidation state and Ce3+/Ce4+ ratio on the Pt/TiO2-CeO2 catalysts in the phenol degradation by catalytic wet air oxidation (CWAO). *Catal. Today* **2015**, *250*, 145−154.
(68) Yang, J.; Ren, S.; Zhang, T.; Su, Z.; Long, H.; Kong, M.; Yao, L. Iron doped effects on active sites formation over activated carbon supported Mn-Ce oxide catalysts for low-temperature SCR of NO. *Chem. Eng. J.* **2020**, *379*, 122398.
(69) Qi, G.; Yang, R. T. A superior catalyst for low-temperature NO reduction with NH3. *Chem. Commun.* **2003**, 848−849.
(70) Hu, H.; Cai, S.; Li, H.; Huang, L.; Shi, L.; Zhang, D. In Situ DRIFTs In″estigation of the Low-Temperature Reaction Mechanism o″er Mn-Doped Co3O4 for the Selecti″e Catalytic Reduction of NOx with NH3. *J. Phys. Chem. C* **2015**, *119* (40), 22924−22933.

https://doi.org/10.1021/acsomega.2c00202
ACS Omega 2022, 7, 12004−12014